

The chiral and angular momentum content of the ρ -meson*

L. Ya. Glozman, C. B. Lang, and M. Limmer

Institut für Physik, FB Theoretische Physik,
Universität Graz, A-8010 Graz, Austria

March 29, 2022

Abstract

It is possible to define and calculate in a gauge-invariant manner the chiral as well as the partial wave content of the quark-antiquark Fock component of a meson in the infrared, where mass is generated. Using the variational method and a set of interpolators that span a complete chiral basis we extract in a lattice QCD Monte Carlo simulation with $n_f = 2$ dynamical light quarks the orbital angular momentum and spin content of the ρ -meson. We obtain in the infrared a simple 3S_1 component as a leading component of the ρ -meson with a small admixture of the 3D_1 partial wave, in agreement with the $SU(6)$ flavor-spin symmetry.

*This paper is dedicated to our colleague Willibald Plessas on occasion of his 60th birthday and will appear in special issue of *Few Body Systems*.

1 Introduction

The $SU(6)_{FS}$ flavor-spin symmetry for the low-lying hadrons in the light flavor sector [1] and its roots (as due to the nonrelativistic quark model [2]) predated QCD and had numerous phenomenological successes. When QCD was established as the fundamental theory of strong interactions it has soon become clear that the current quarks of QCD in the u, d sector have tiny masses, of the order of a few MeV at the renormalization scale of 1-2 GeV. They are very far away from the rather heavy constituent quarks of the quark model. In view of this the QCD Lagrangian has approximate chiral symmetry.

At the same time it was clear that this approximate chiral symmetry is dynamically broken in the vacuum and this breaking is a source of mass of the low-lying hadrons. Different microscopical models (with varying definitions of the quark mass) exist for chiral symmetry breaking in the vacuum and they indicate that indeed at large space-like momenta the quark mass matches its bare values of a few MeV, while at low momenta it runs to the value of the constituent quark mass in the definitions given by the models. There also exist lattice determinations of such masses at low momenta, see, e.g., [3, 4], though such determinations are manifestly gauge dependent. By fixing a gauge and considering a single quark propagator in the background gluonic field it is not clear a priori how the confining gluodynamics (that drives the dynamics in the color-singlet hadrons) is taken into account. Then it is interesting to see how it would be possible to provide a bridge from QCD in the infrared to the language of the quark model in a model-independent and gauge-invariant manner.

There is a systematic method to study the hadron composition on the lattice - the variational method [5, 6]. In that approach one selects a set of interpolating operators $\{O_1, O_2, \dots, O_N\}$ with the proper quantum numbers that couple to a given hadron. One computes the cross-correlation matrix

$$C_{ij}(t) = \langle O_i(t) O_j^\dagger(0) \rangle. \quad (1)$$

Masses of the ground and excited states of hadrons with fixed quantum numbers can be extracted from the t -dependence of the eigenvalues of this matrix at large Euclidean times t . If the set of operators O_i is complete enough, then the eigenvectors represent the “wave function” of the hadron (see the cautionary remarks at the begin of Sect. 4 and the definition (19)). Of course, hadrons contain many different Fock components. Our task is to reconstruct

the leading one, the quark-antiquark component of the low-lying mesons. For this one needs a set of operators that allows one to define uniquely such a component. This set of operators must be complete in the $\bar{q}q$ space with regard to the chiral basis.

All possible $\bar{q}q$ interpolators for non-exotic mesons in the u, d sector have been classified according to transformation properties with respect to $SU(2)_L \times SU(2)_R$ and $U(1)_A$ chiral groups [7, 8]. If one assumes that there is no explicit excitation of the gluonic field with the non-vacuum quantum numbers, which is certainly true for low-lying hadrons, then the $SU(2)_L \times SU(2)_R$ representations for the quark-antiquark system specify a complete and orthogonal basis. Consequently a set of interpolators that is in one-to-one correspondence with all possible chiral representations of $SU(2)_L \times SU(2)_R$ is a complete one and can be used to define the $\bar{q}q$ component of a meson. The cross-correlation matrix with such a set can be used to reconstruct the $\bar{q}q$ Fock component. The eigenvectors of this correlation matrix represent the $\bar{q}q$ content in terms of different chiral representations. Observing a superposition of different chiral representations implies that chiral symmetry is broken.

It turns out that it is also possible to reconstruct a composition of the $\bar{q}q$ component in terms of the $^{2S+1}L_J$ basis, where $\mathbf{J} = \mathbf{L} + \mathbf{S}$ are standard angular momenta. Indeed, the complete and orthogonal chiral basis can be related, through a unitary transformation, to the complete and orthogonal $^{2S+1}L_J$ basis in the center-of-momentum frame [9]. Then diagonalizing the cross-correlation matrix with interpolators that span a complete set of chiral representations and using this unitary transformation to the $^{2S+1}L_J$ basis one can obtain from the eigenvectors of the correlation matrix a partial wave decomposition of the $\bar{q}q$ component.

In QCD the decomposition of a hadron should depend on the scale at which we probe this hadron. In other words, what we see in our microscope depends on the resolution. In our case “the microscope” is our interpolating operator O_i that creates the hadron from the vacuum. A true point-like source would correspond to the point-like lattice interpolator in the limit of the lattice spacing approaching 0, $a \rightarrow 0$. The point-like interpolator applied on the lattice with the spacing a probes the hadron at the scale specified by a . In the continuum limit it becomes the true point-like operator and probes the hadron at the scale $\mu^2 \rightarrow \infty$. Here we want to study the hadron structure at the infrared scale, where the mass is generated. This scale is determined by the hadron size, of the order 0.3 - 1 fm. In lattice simulations

we cannot use such a large a , because then the lattice artifacts are too large and matching to continuum theory is lost. However, such a low scale can be fixed by the gauge-invariant smearing of the interpolators. If we use the interpolating operator smeared over the size R in the physical units such that $R/a \gg 1$, then even in the continuum limit $a \rightarrow 0$ we probe the hadron structure at the scale R . Changing the smearing size R we can study the hadron content at different scales of the continuum theory at $a \rightarrow 0$.

In this paper we expand our results on the chiral and partial wave decomposition of the ρ -meson in the infrared, presented in a recent letter [10], discuss all required details of the formalism and physical interpretation as well as give some additional numerical results.

2 Chiral classification of the quark-antiquark interpolators

The chiral classification of some of the $\bar{q}q$ interpolators was done in [11]. A complete classification was performed in [7, 8] and is summarized here.

We consider the two-flavor mesons. All quark-antiquark bilinear operators in the chiral limit can be classified according to the representations of the $SU(2)_L \times SU(2)_R$ and $U(1)_A$ chiral groups. Consider, as example, local interpolators of $J = 0$ mesons, built from quark isodoublets q :

$$O_\pi(x) = i \bar{q}(x) \vec{\tau} \gamma_5 q(x) , \quad (2)$$

$$O_{f_0}(x) = \bar{q}(x) q(x) , \quad (3)$$

$$O_\eta(x) = i \bar{q}(x) \gamma_5 q(x) , \quad (4)$$

$$O_{a_0}(x) = \bar{q}(x) \vec{\tau} q(x) , \quad (5)$$

where $\vec{\tau}$ denotes the vector of isospin Pauli matrices. The $SU(2)_L \times SU(2)_R$ transformations consist of vectorial and axial transformations in the isospin space. The axial transformation mixes the currents of opposite parity:

$$O_\pi(x) \leftrightarrow O_{f_0}(x) \quad (6)$$

as well as

$$O_{a_0}(x) \leftrightarrow O_\eta(x). \quad (7)$$

Hence the currents (6) form the basis functions of the $(1/2, 1/2)_a$ representation of the chiral $SU(2)_L \times SU(2)_R$ while the interpolators (7) transform as $(1/2, 1/2)_b$.

Table 1: The complete set of $\bar{q}q$ states (interpolators) classified according to the chiral basis. The symbol \leftrightarrow indicates the states (interpolators) belonging to the same representation of $SU(2)_L \times SU(2)_R$.

R	$J = 0$	$J = 1, 3, \dots$	$J = 2, 4, \dots$
$(0, 0)$	—	$0J^{++} \leftrightarrow 0J^{--}$	$0J^{--} \leftrightarrow 0J^{++}$
$(1/2, 1/2)_a$	$1J^{-+} \leftrightarrow 0J^{++}$	$1J^{+-} \leftrightarrow 0J^{--}$	$1J^{-+} \leftrightarrow 0J^{++}$
$(1/2, 1/2)_b$	$1J^{++} \leftrightarrow 0J^{-+}$	$1J^{--} \leftrightarrow 0J^{+-}$	$1J^{++} \leftrightarrow 0J^{-+}$
$(0, 1) \oplus (1, 0)$	—	$1J^{--} \leftrightarrow 1J^{++}$	$1J^{++} \leftrightarrow 1J^{--}$

As another example consider local interpolators of the ρ -meson. There exist two different bilinear operators with the ρ -meson quantum numbers that have radically different chiral transformation properties. The first one is the standard vector current,

$$O_\rho^V(x) = \bar{q}(x) \gamma^i \vec{\tau} q(x) , \quad (8)$$

and the second one is the pseudotensor operator,

$$O_\rho^T(x) = \bar{q}(x) \sigma^{0i} \vec{\tau} q(x). \quad (9)$$

The axial $SU(2)_L \times SU(2)_R$ transformation mixes the vector current with the axial vector current,

$$O_{a_1}(x) = \bar{q}(x) \gamma^i \gamma^5 \vec{\tau} q(x), \quad (10)$$

while the pseudotensor interpolator gets mixed with the interpolator of the h_1 meson,

$$O_{h_1}(x) = \varepsilon^{ijk} \bar{q}(x) \sigma^{jk} q(x). \quad (11)$$

Consequently the operators

$$O_\rho^V(x) \leftrightarrow O_{a_1}(x) \quad (12)$$

form a basis of the $(0, 1) \oplus (1, 0)$ representation of $SU(2)_L \times SU(2)_R$, while the interpolators

$$O_\rho^T(x) \leftrightarrow O_{h_1}(x) \quad (13)$$

transform as $(1/2, 1/2)_b$. A complete set of representations of $SU(2)_L \times SU(2)_R$ and the corresponding quantum numbers are listed in Table 1.

In Table 1 the index R determines a representation of the $SU(2)_L \times SU(2)_R$ with $R = (0, 0)$, $(1/2, 1/2)_a$, $(1/2, 1/2)_b$, or $(0, 1) \oplus (1, 0)$. All states (interpolators) are uniquely specified by the set of quantum numbers $\{R; IJ^{PC}\}$ where we use the standard notations for the isospin I , total spin J as well as for the spatial and charge parities PC . The chiral basis $\{R; IJ^{PC}\}$ is obviously consistent with Poincaré invariance. The symbol \leftrightarrow indicates that both given states (interpolators) are members of a particular chiral multiplet, that is they transform into each other upon $SU(2)_L \times SU(2)_R$.

For a particle with the ρ -meson quantum numbers the $(0, 1) \oplus (1, 0)$ and the $(1/2, 1/2)_b$ representations are a complete set. Both interpolators, O_ρ^V and O_ρ^T , may create the ρ -meson from the vacuum. If both couple, indeed, this signals chiral symmetry breaking.

3 Transformation from the chiral to the angular momentum basis

The chiral basis can be related, through a unitary transformation, to the $\{I; {}^{2S+1}L_J\}$ basis in the center-of-momentum frame [9]:

$$|R; IJ^{PC}\rangle = \sum_L \sum_{\lambda_q \lambda_{\bar{q}}} \chi_{\lambda_q \lambda_{\bar{q}}}^{RPI} \sqrt{\frac{2L+1}{2J+1}} C_{\frac{1}{2}\lambda_q \frac{1}{2}-\lambda_{\bar{q}}}^{S\Lambda} C_{L0S\Lambda}^{J\Lambda} |I; {}^{2S+1}L_J\rangle, \quad (14)$$

where the summation is implied in helicities of the fermion λ_q and antifermion $\lambda_{\bar{q}}$ as well as in the orbital angular momenta L such that $(-1)^{L+1} = P$. The total spin S is fixed by the quantum numbers IJ^{PC} . Coefficients $\chi_{\lambda_q \lambda_{\bar{q}}}^{RPI}$ can be extracted from Table 2 of Ref. [9]. It follows immediately from Eq. (14) that every state (interpolator) in the chiral basis is a fixed (prescribed by chiral symmetry and unitarity) superposition of allowed states in the $\{I; {}^{2S+1}L_J\}$ basis. For instance, there are two kinds of the vector states (interpolators) with the quantum numbers of the ρ -meson, which are represented by two orthogonal fixed combinations of S - and D -waves:

$$\begin{pmatrix} |(0, 1) \oplus (1, 0); 1 \ 1^{--}\rangle \\ |(1/2, 1/2)_b; 1 \ 1^{--}\rangle \end{pmatrix} = U \cdot \begin{pmatrix} |1; {}^3S_1\rangle \\ |1; {}^3D_1\rangle \end{pmatrix} \quad (15)$$

with

$$U = \begin{pmatrix} \sqrt{\frac{2}{3}} & \sqrt{\frac{1}{3}} \\ \sqrt{\frac{1}{3}} & -\sqrt{\frac{2}{3}} \end{pmatrix}. \quad (16)$$

In terms of the quark-antiquark bilinears the state $|(0, 1) \oplus (1, 0); 1 \ 1^{--}\rangle$ is given by the spatial components of the standard vector current, O_ρ^V from (8), while the pseudotensor interpolator O_ρ^T in (9) represents $|(1/2, 1/2)_b; 1 \ 1^{--}\rangle$.

¹ Consequently, diagonalizing the cross-correlation matrix with the O_ρ^V and O_ρ^T interpolators and using the unitary transformation we can reconstruct the partial wave content of the $\bar{q}q$ component of the ρ -meson.

4 The variational method and the “wave function” of a hadron

The composition of hadronic states in quantum field theory is a subtle issue. Whereas in non-relativistic approaches the notion of a wave function and a complete basis of states is well-defined, in QFT beyond the ground state there is no well-defined single hadron, the state is always a scattering state with superposition of many particle components. A given hadron interpolator couples in principle to all states with its quantum numbers.

In the lattice formulations this situation is further complicated by the coarseness of the lattice and its symmetries, which mostly have no one-to-one correspondence to the continuous space-time symmetries. Lattice interpolators for mesons, in their simplest disguise, are point like or extended color singlet quark-antiquark combinations with suitable combination of their Dirac components.

Combinations of such interpolators may then be formed such as to represent lattice analogues of spin representations [12, 13]. Usually the even or odd spin representations mix among them, thus, e.g., a lattice interpolator representing a $J = 1$ vector will have contributions which correspond to higher odd J states and thus corresponding signals in the correlation function. Suitable combinations may improve the situation, but much higher statistics is then necessary. This is one of the reasons why lattice studies of excited states are progressing slowly.

¹It is actually possible to construct interpolators with derivatives that also transform according to the representations above [7, 8].

The variational method [5, 6] (for a recent, more complete set of references cf. [14]) provides a method to find the optimal combinations. Starting with a set of interpolators $\{O_1, O_2, \dots, O_N\}$ one determines the correlation function (1) and solves a generalized eigenvalue problem (see below). Given a large enough basis set of interpolators the eigenvalues may then be related to the eigenstates of the Hamiltonian and the corresponding energy values.

In order to avoid possible prejudices one should provide a large basis of interpolators. On the other hand, using too many such interpolators may increase the statistical noise in the analysis. Since the optimal combination models the hadron structure it is helpful to be guided by intuition – which is, however, another word for prejudice. Thus the selection of a suitable basis is close to being an art and one has to balance quality with quantity.

The normalized physical states $|n\rangle$ propagate in time with

$$\langle n(t)|m(0)\rangle = \delta_{nm}e^{-E^{(n)}t}. \quad (17)$$

The interpolating (lattice) operators $O_i(t)$ are projected to vanishing spatial momentum and are usually not normalized.

We compute the correlation function

$$C(t)_{ij} = \langle O_i(t)O_j^\dagger(0)\rangle = \sum_n^\infty a_i^{(n)}a_j^{(n)*}e^{-E^{(n)}t}, \quad (18)$$

with the coefficients giving the overlap of the lattice operator with the physical state,

$$a_i^{(n)} = \langle 0|O_i|n\rangle. \quad (19)$$

For interpolating operators O_i spanning an orthogonal basis these values would indeed constitute the wave function of state $|n\rangle$ in that basis (more exactly, the Bethe-Salpeter amplitude). In this work we are using the term “wave function” for this matrix element.

We assume that the correlation matrix (18) can be approximated by a finite sum over N states and denote this approximation by

$$\hat{C}(t)_{ij} = \sum_{n=1}^N a_i^{(n)}a_j^{(n)*}e^{-E^{(n)}t}. \quad (20)$$

The eigenvector and eigenvalues of \hat{C} will not exactly agree with those of C .

It can be shown [5, 6] (for a recent discussion see [15, 14]) that the generalized eigenvalue problem (summation convention)

$$\hat{C}(t)_{ij}u_j^{(n)} = \lambda^{(n)}(t, t_0)\hat{C}(t_0)_{ij}u_j^{(n)} \quad (21)$$

allows to recover the correct eigensystem approximately, i.e.,

$$\lambda^{(n)}(t, t_0) = e^{-E^{(n)}(t-t_0)} \left(1 + \mathcal{O} \left(e^{-\Delta E^{(n)}(t-t_0)} \right) \right) . \quad (22)$$

Here $\Delta E^{(n)}$ may be as small as the distance to the next nearby energy level. In [14] it was pointed out that in an interval $t_0 \leq t \leq 2t_0$ these contributions are suppressed and leading terms even have $\Delta E^{(n)}$ equal to the distance to the first neglected energy level $E^{(N+1)}$. At t_0 all eigenvalues are 1 and the eigenvectors are arbitrary.

Inserting (20) into (21) one sees that the eigenvectors of the generalized eigenvalue problem come out orthogonal to the original wave functions $a^{(n)}$,

$$(u^{(n)}, a^{(m)}) \equiv \sum_{i=1}^N u_i^{(n)*} a_i^{(m)} = c^{(m)} \delta_{nm} , \quad (23)$$

and approximate the correct ones. The normalizing factor $c^{(m)}$ we can get rid off.

Defining a sum of lattice operators

$$\eta^{(n)} \equiv \sum_{i=1}^N u_i^{(n)*} O_i , \quad (24)$$

we find

$$\langle m | \eta^{(n)} | 0 \rangle = \sum_{i=1}^N u_i^{(n)*} \langle 0 | O_i^\dagger | m \rangle = \sum_{i=1}^N u_i^{(n)*} a_i^{(m)} = c^{(n)} \delta_{nm} . \quad (25)$$

Therefore η creates a physical state,

$$\eta^{(n)\dagger} | 0 \rangle = c^{(n)*} | n \rangle . \quad (26)$$

The eigenvector coefficients give the composition of the eigenstate in terms of the (non-orthogonal) interpolating operators:

$$a_i^{(n)} = \langle 0 | O_i | n \rangle = \frac{1}{c^{(n)*}} \langle 0 | O_i \eta^{(n)\dagger} | 0 \rangle = \frac{1}{c^{(n)*}} \sum_{j=1}^N u_j^{(n)} \langle 0 | O_i O_j^\dagger | 0 \rangle . \quad (27)$$

They would agree with $u_j^{(n)}$ if the interpolators were orthogonal, which they are usually not.

The eigenvectors of the generalized eigenvalue problem for hermitian matrices $\hat{C}(t)$, $\hat{C}(t_0)$ obey the orthogonality relation

$$\left(u^{(n)}, \hat{C}(t)u^{(n)}\right) \propto \delta_{nm} . \quad (28)$$

Indeed, with (18) and (23) we find for large t (summation convention)

$$\begin{aligned} w_i^{(n)}(t) &\equiv \hat{C}(t)_{ij}u_j^{(n)} \sim c^{(n)*}a_i^{(n)}e^{-E^{(n)}t} , \\ \left(u^{(n)}, w^{(n)}\right) &= u_i^{(n)*}\hat{C}(t)_{ij}u_j^{(n)} = c^{(n)*}u_i^{(n)*}a_i^{(n)}e^{-E^{(n)}t} \\ &= \left|c^{(n)}\right|^2 e^{-E^{(n)}t} , \end{aligned} \quad (29)$$

and for the ratio

$$\frac{\left|w_i^{(n)}\right|^2}{\left(u^{(n)}, w^{(n)}\right)} = \left|a_i^{(n)}\right|^2 e^{-E^{(n)}t} . \quad (30)$$

Assuming asymptotically leading exponential behavior this allows to read off $|a_i^{(n)}|$ in the asymptotic region. Ideally $a_i^{(n)}$ should not depend on t , in actual calculations, however, one identifies a region of t -value where it is compatible with a constant.

We may utilize this result to determine ratios of couplings of the different lattice operators to the physical states,

$$\frac{w_i^{(n)}(t)}{w_k^{(n)}(t)} = \frac{\hat{C}(t)_{ij}u_j^{(n)}}{\hat{C}(t)_{kj}u_j^{(n)}} = \frac{a_i^{(n)}}{a_k^{(n)}} . \quad (31)$$

One computes the ratio for several values of t and identifies its value in a plateau region. The ratio tells us how much different interpolating operators contribute to the eigenstate $|n\rangle$. This can be used to discuss contributions of, e.g., different representations of the vector meson channel, as we do here.

In a realistic simulation many physical states may contribute and one has to use the discussed techniques to single out couplings to the state of interest. In some approximation one may instead look just at the ratios of individual entries of the correlation matrix, like

$$\hat{C}_{ii}(t)/\hat{C}_{jj}(t) \quad \text{or} \quad \hat{C}_{ii}(t)/\hat{C}_{ij}(t) \quad (32)$$

in the asymptotic t -region, where the excited states contributions are suppressed [16, 17, 18].

The ratio

$$\left| \frac{a_i^{(n)}}{a_i^{(m)}} \right|^2 = \left| \frac{\langle 0 | O_i(t) | n \rangle}{\langle 0 | O_i(t) | m \rangle} \right|^2 \quad (33)$$

tells us how much the interpolating operator O_i contributes to the eigenstates $|n\rangle$ and $|m\rangle$. This can be used to discuss the ratio of decay constants of various excitations as done in [19, 15, 14].

5 Vector meson couplings for local interpolators

Here we quote definitions of the local coupling constants of the vector and pseudotensor currents to the ρ -meson in continuum and discuss their relations to the matrix elements obtained in the previous section.

In Minkowski space the corresponding amplitudes are given as

$$\langle 0 | \bar{q}(0) \gamma^\mu q(0) | V(p; \lambda) \rangle = m_\rho f_\rho^V e_\lambda^\mu, \quad (34)$$

$$\langle 0 | (\bar{q}(0) \sigma^{\alpha\beta} q(0)) (\mu) | V(p; \lambda) \rangle = i f_\rho^T(\mu) e_\lambda^\mu (e_\lambda^\alpha p^\beta - e_\lambda^\beta p^\alpha). \quad (35)$$

Here $V(p; \lambda)$ is the vector meson state with the mass m_ρ , momentum p and polarization λ . The vector current is conserved, consequently the vector coupling constant f_ρ^V is scale-independent. The pseudotensor “current” is not conserved and is subject to a nonzero anomalous dimension. Consequently the pseudotensor coupling $f_\rho^T(\mu)$ manifestly depends on the scale μ . In the rest frame the ratio

$$\frac{f_\rho^V}{f_\rho^T(\mu)} = \frac{\langle 0 | \bar{q}(0) \gamma^i q(0) | V(\lambda) \rangle}{\langle 0 | (\bar{q}(0) \sigma^{0i} q(0)) (\mu) | V(\lambda) \rangle} \quad (36)$$

coincides with the ratio of matrix elements (31).

That ratio can be extracted from the ratio of the vector-vector and pseudotensor-vector zero-momentum correlators at large Euclidean times, when the excited states do not contribute any more. If the source is located at the point $(t, \vec{x}) = (0, \vec{0})$ and the sink is at the arbitrary point (t, \vec{x}) , then

at large t one obtains asymptotically

$$\begin{aligned} \sum_{\vec{x}} \langle 0 | \left(\bar{q}(t, \vec{x}) \gamma^i q(t, \vec{x}) \right) \left(\bar{q}(0) \gamma^i q(0) \right)^\dagger | 0 \rangle &\sim (f_\rho^V)^2 m_\rho^2 \exp(-m_\rho t) , \quad (37) \\ \sum_{\vec{x}} \langle 0 | \left(\bar{q}(t, \vec{x}) \sigma^{0i} q(t, \vec{x}) \right) (\mu) \left(\bar{q}(0) \gamma^i q(0) \right)^\dagger | 0 \rangle &\sim f_\rho^V f_\rho^T(\mu) m_\rho^2 \exp(-m_\rho t) \quad (38) \end{aligned}$$

The ratio of these correlators is equal to the ratio $f_\rho^V / f_\rho^T(\mu)$. With the variational method the ground state can be identified already at small Euclidean time distance and thus the quality of the result can be improved, see Sect. 7.

In [16, 17, 18] this ratio has been used to extract $f_\rho^V / f_\rho^T(\mu)$ and to relate² it to the continuum $\overline{\text{MS}}$ -scheme at a scale of 2 GeV. While this method is suitable to study the ratio for the ground state and the result agrees with that extracted from the variational method (to be compared later on), only the variational method can be used to study such ratios for excited states.

6 Smearing of the interpolators and the resolution scale

So far we discussed the cross-correlation matrix as obtained with the local interpolators. In lattice simulations the hadron interpolators can be built with different spatial extent, e.g., using so-called smeared quark sources. For example, an isovector interpolator may have the form

$$\bar{d}(x') S_{x'0}^\dagger \Gamma S_{0x''} u(x'') , \quad (39)$$

where we omit the Dirac indices; Γ denotes some Dirac matrix and S_{xy} is some gauge transporter from y to x . For the local interpolator at the origin one has $x' = x'' = 0$. Summation over x' and x'' may be used to define quark source smearing, thus improving the signal when computing correlators of such interpolators.

²Here there is a subtle point. In the $\overline{\text{MS}}$ -scheme of continuum theory one uses a renormalization group equation obtained to typically two or three loops to relate the ratio at different scales. Such a renormalization group equation cannot adequately represent the physics related to chiral symmetry breaking, because chiral symmetry breaking is intrinsically a nonperturbative effect. If, at given scale, the ρ -meson couples strongly to both, vector and pseudotensor interpolators, then chiral symmetry is strongly broken in the ρ -meson at that scale. If chiral symmetry is broken, however, it is unclear whether perturbative RG is applicable to relate the ratio $f_\rho^V / f_\rho^T(\mu)$ at different scales.

One purpose of such a smearing is to improve the quality of the signal from the state of interest in order to extract, e.g., its mass. Indeed, with the local interpolator the coupling of this interpolator to the physical state is determined by the behavior of this state at the origin. With the local interpolators we therefore probe the hadron wave function at the scale fixed by the lattice spacing a . If we smear the local interpolator in a gauge-invariant way over a spatial region of size R , then the coupling of our interpolator to the physical state may be better and the quality of the signal is improved. So the smearing typically plays a technical role. In our case, however, we give the smearing width a fundamental role – it defines a resolution scale at which we study the hadron wave function. Of course, different smearing methods may lead to different definitions.

Only a few quantities in QCD do not depend on the scale. For example, the lattice spacing a fixes the ultraviolet cut-off (i.e., the renormalization scale), and the observables such as the ratios of masses of different hadrons, their electric charges should not depend on this scale. Most of the quantities in QCD do depend on the resolution scale at which they are studied. We want to study the hadron wave function in the infrared (where mass is generated), i.e., at the very low resolution scale characterized by the typical hadron size. Certainly we cannot chose a to be so large since then we lose matching to the ultraviolet (continuum) limit of QCD. However, even if we use a reasonably small a we can fix a scale where we study the hadron at the smearing size R . If $R \gg a$, it is the size of the smearing R that defines a resolution scale where we probe the hadron properties. Consequently, the smearing plays a rather fundamental role – it defines a scale at which we study the content of our hadron. Physically it means that given a source smearing size R , we cannot resolve details of our wave function with the smaller size. Physical (continuum) results can be deduced from the extrapolation to the $a = 0$ point while keeping R fixed in physical units.

We fix the resolution scale in the following way. We substitute a local interpolator at the point (t, \vec{x}) by the interpolator with the same quantum numbers but with quark fields smeared in spatial coordinates over the size R in a gauge-invariant way around the point (t, \vec{x}) . The profile of the smeared quark fields should be approximately Gaussian with the width R . Therefore we use the so-called Jacobi smearing [20, 21]. A point-like source S_0 is

smeared out by acting with a smearing operator M ,

$$S = MS_0, \quad M = \sum_{n=0}^N (\kappa H)^n, \quad (40)$$

where H is a hopping term,

$$H = \sum_{\hat{j}=1}^3 \left[U_{\hat{j}}(\vec{x}, t) \delta_{\vec{x}+\hat{j}, \vec{y}} + U_{\hat{j}}^\dagger(\vec{x} - \hat{j}, t) \delta_{\vec{x}-\hat{j}, \vec{y}} \right]. \quad (41)$$

The smearing extends only over individual time slices, i.e., t is fixed. The parameters κ (hopping parameter) and N (number of smearing steps) are tuned to get an approximately Gaussian shape of the quark source with a certain width R in physical units. Different smearing algorithms may be used for different definitions of the resolution scale.

7 Simulation details and results

In earlier work we have studied so-called chirally improved (CI) fermions [22, 23] in the quenched [24, 25, 26, 13] and the dynamical [27] case for two mass-degenerate light quarks. The gauge field action was the tadpole improved Lüscher-Weisz action [28]. Table 2 gives some information on the runs analyzed here, details on the simulation and other observables (e.g., hadron masses) can be found in the original papers. The spatial lattice size 16 corresponds to a physical size close to 2.4 fm, the temporal size is twice as large.

In the quenched simulations the ρ cannot decay; in our dynamical ensembles [27] its mass is also above the decay threshold since extra units of relative (quantized lattice) momentum are needed for the decay. Below threshold the 2-pion states will become important and probably modify our results. However, we study here only the quark-antiquark contributions to the ρ lattice state. Adding further, more-quark interpolators may affect the overall normalization of the quark-antiquark component but is unlikely to change the ratios of the vector vs. pseudovector operators of the quark-antiquark contribution. Only this ratio is important for the partial wave decomposition.

In our analysis we use the variational method, with quark-bilinear meson interpolators. We use Jacobi smearing of quark sources with the values for κ and N such as to obtain a narrow (index n) and a wide (index w) source

Table 2: Specification of the data used here; for the gauge coupling only the leading value β_{LW} is given, m_0 denotes the bare mass parameter of the CI-action. Further details like the determination of the lattice spacing and the π - and ρ -masses are found in [13, 27]. For the quenched case and for the dynamical ensemble A we used 100 configurations, for sets B and C we analyzed 200 configurations each. The lattice size is $16^3 \times 32$ throughout.

Data	β_{LW}	$a m_0$	a [fm]	m_π [MeV]	m_ρ [MeV]
Quenched	7.90	0.04–0.20	0.1480(10)	475–1053	912–1251
dyn.: A	4.70	-0.050	0.1507(17)	526(7)	922(17)
dyn.: B	4.65	-0.060	0.1500(12)	469(4)	897(13)
dyn.: C	4.58	-0.077	0.1440(12)	318(5)	810(28)

with effective smearings widths [25] of 0.27 fm and 0.41 fm for the quenched ensembles and 0.27 fm and 0.55 fm for the dynamical ones, respectively [13, 27].

The variational method not only allows to identify the excited state(s) – depending on the number of interpolators used and the statistical quality of the data – but also gives increased stability in the ground state signal. Here we discuss only results obtained for the ground state in the isovector vector channel, the ρ -meson ($J^{PC} = 1^{--}$). We include the operators

$$\begin{aligned}
O_n^V &= \bar{u}_n \gamma^i d_n, & O_w^V &= \bar{u}_w \gamma^i d_w, & O_p^V &= \bar{u}_p \gamma^i d_p, \\
O_n^T &= \bar{u}_n \gamma^t \gamma^i d_n, & O_w^T &= \bar{u}_w \gamma^t \gamma^i d_w, & O_p^T &= \bar{u}_p \gamma^t \gamma^i d_p,
\end{aligned} \tag{42}$$

where γ^i is one of the spatial Dirac matrices, γ_t is the γ -matrix in (Euclidean) time direction, and the subscripts w and n denote the two smearing widths of the quark sources, whereas p indicates point quark sources. We denote the ratios of the coupling of the ρ -meson to the different interpolators by $[a_\rho^V/a_\rho^T](n)$ for the narrow quark sources and analogously for the other two cases w and p .

In Fig. 1 we compare the ratios (which we call a-ratios henceforth) of the coefficients determined from diagonalization of the correlation matrix between interpolators O_n^V , O_w^V , O_n^T , O_w^T as discussed in (31) with the direct ratio between matrix elements (called d-ratios) according to (32).

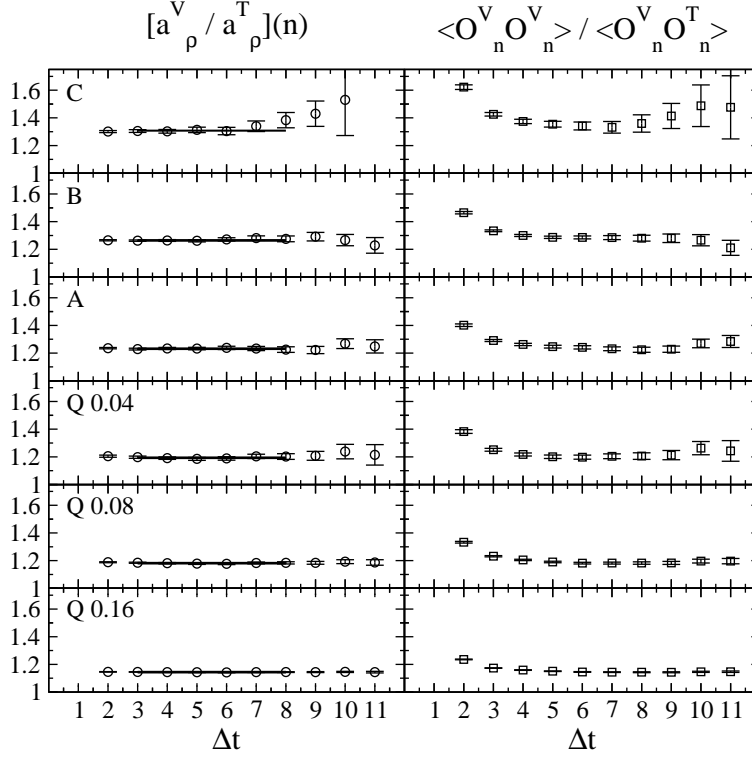


Figure 1: We compare for a_ρ^V / a_ρ^T the a-ratios (left-hand column) determination with the d-ratio (right-hand column) determination for dynamical and some quenched data sets. The error bars have been determined with single-elimination jack-knife. The horizontal lines indicate the plateau fit range and value used in Fig. 3. The data correspond to ensembles given in Table 2, for the quenched ensemble we show only the results for valence masses 0.04, 0.08 and 0.16 (in lattice units).

The plateaus of the a-ratios are remarkable wide and stable for large quark masses and decrease in quality towards smaller masses. However, even for run C with m_π close to 320 MeV we still observe good quality plateaus for time separations $\Delta t = 3 \dots 8$. The direct d-ratios have larger errors and much worse plateau behavior; for run C only the range $\Delta t = 5 \dots 8$ is acceptable. The contamination with excited states at smaller distances is obvious. The values are, however, compatible with the a-ratios. We also confirm that, e.g., the d-ratios $\langle O_n^V O_n^V \rangle / \langle O_n^T O_n^T \rangle$ are approximately equal to $\left(\langle O_n^V O_n^V \rangle / \langle O_n^V O_n^T \rangle \right)^2$.

The data for the wide sources are qualitatively similar. We therefore use the a-ratio averages of the plateau values from 3 to 8 as our value estimate for $[a_\rho^V/a_\rho^T](n)$ for the narrow sources and $[a_\rho^V/a_\rho^T](w)$ for the wide sources.

The quark-propagators for point sources were not available but we do have correlation matrix entries between smeared source interpolators and point sink interpolators. Due to that limitation we cannot use the variational method (we do not have the full correlation matrix) but determine the results via d-ratios of entries of the correlation matrix giving $[a_\rho^V/a_\rho^T](p)$.

In the ratios

$$\left(\langle O_n^V O_p^V \rangle / \langle O_n^V O_p^T \rangle \right)^2 \quad \text{and} \quad \left(\langle O_w^V O_p^V \rangle / \langle O_w^V O_p^T \rangle \right)^2 \quad (43)$$

ideally the effect of the smeared sources should cancel and the ratios should agree. In Fig. 2 we compare them and find agreement in the plateau region, which, however is shrinking and hardly identifiable for the run C with smallest quark mass. It is interesting to note that the wide source ratios appear to have less contamination from excited states. We use these for the values in Fig. 3.

Fig. 3 exhibits our results for $[a_\rho^V/a_\rho^T]$ for all three situations of interpolator smearing: w , n and p comparing quenched with dynamical data. A systematic dependence on the smearing scale of the interpolators is obvious. We also find that towards smaller quark masses the quenched results (i.e., for the lowest valence masses 0.04 and 0.06 in lattice units) significantly deviate from the data with dynamical quarks.

We observe a clear and systematic dependence of a_ρ^V/a_ρ^T on the smearing properties of the hadron interpolators, more precisely: the quark sources building the interpolators. As discussed in Sect. 6 the dependence on the smearing width (ranging from 0.55 fm down to the unsmeared point scale $a \approx 0.15$ fm) allows to relate the composition of the ρ on various infrared

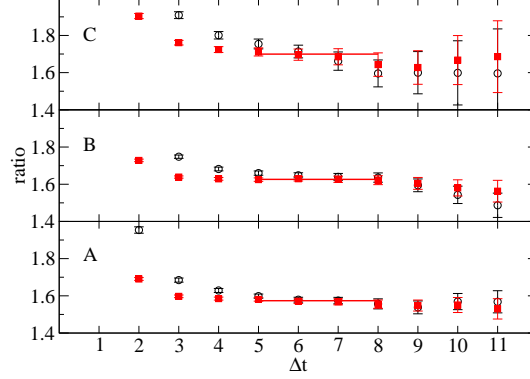


Figure 2: We compare (for the dynamical data runs A, B and C) ratios of correlation matrix entries (see (43)), which in the plateau region should give $[a_\rho^V/a_\rho^T](p)$. The results for narrow (open symbols) and wide (full symbols) sources agree in the plateau region, but the plateau range shrinks and is hardly justifiable for run C. The error bars have been determined with single-elimination jack-knife. The horizontal lines indicate the plateau fit range (for the w sources) and the fit value used in Fig. 3.

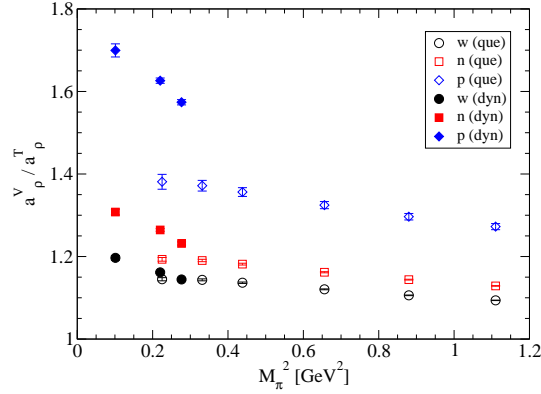


Figure 3: We compare our results for $[a_\rho^V/a_\rho^T]$ for the three smearing scales: w , n and p (no smearing). The open symbols denote quenched data, the full symbols the data with dynamical quarks. The error bars have been determined with single-elimination jack-knife.

resolution scales. A more systematic study of that scale dependence may allow to better compare with effective models.

Physically the ratio encodes how the chiral symmetry is broken in the (quark-antiquark components of the) ρ wave function at different scales. The $(0, 1) \oplus (1, 0)$ (i.e., the vector) and the $(\frac{1}{2}, \frac{1}{2})_b$ (i.e., the pseudotensor) representations are a complete set for the $\bar{q}q$ component of the ρ -meson. Hence, chiral symmetry is broken in the ρ wave function such that the $\bar{q}q$ component is a superposition of both with a relative ratio shown in Fig. 3. There we see clear evidence for the resolution scale dependence of chiral symmetry breaking. Extrapolating to physical quark masses (where we have to assume that opening the 2-pion decay channel would not affect the result significantly) we expect that the ratio varies from ≈ 1.75 for point interpolators (a resolution scale given by the lattice spacing $a \approx 0.15$ fm) down to ≈ 1.25 for the interpolators built with smeared, wide quark sources, where the resolution scale is given from the smearing width $R \approx 0.55$ fm.

Inverting the unitary transformations (15)–(16) we conclude that the $\bar{q}q$ component of the ρ -meson is varying from predominantly 3S_1 wave for the large R values with increasing admixture of 3D_1 towards smaller R , e.g.,

$$\begin{aligned} \frac{a_\rho^V}{a_\rho^T} = 1.75 &\rightarrow 0.995|1; ^3S_1\rangle + 0.096|1; ^3D_1\rangle, \\ \frac{a_\rho^V}{a_\rho^T} = \sqrt{2} &\rightarrow |1; ^3S_1\rangle, \\ \frac{a_\rho^V}{a_\rho^T} = 1.25 &\rightarrow 0.998|1; ^3S_1\rangle - 0.059|1; ^3D_1\rangle. \end{aligned} \quad (44)$$

In Fig. 4 we show the inverse ratio a_ρ^T/a_ρ^V . Towards $\mu \sim 1/R \rightarrow \infty$ the pseudotensor contribution decouples from the ρ -meson, $f_\rho^T(\mu \rightarrow \infty) = 0$, as follows from renormalization group behavior [16] in the asymptotic freedom regime. Hence the inverse ratio should approach 0 for $R \rightarrow 0$, fully compatible with Fig. 4. At this point the partial wave decomposition is determined by the $(0, 1) \oplus (1, 0)$ representation alone. For large R the inverse ratio saturates with the 3S_1 partial wave strongly dominating over 3D_1 , with little dependence on the quark (or pion) mass.

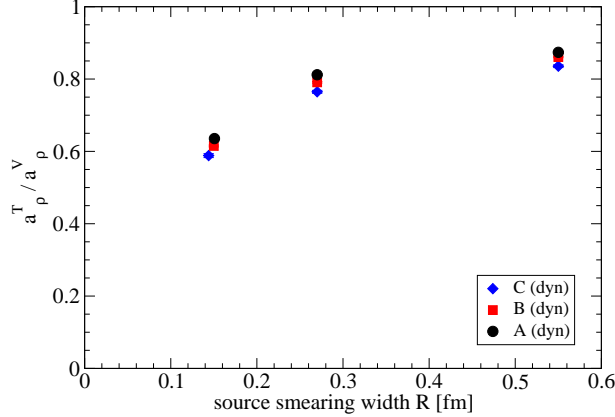


Figure 4: We show the dependence of $[a_\rho^T/a_\rho^V]$ on the width of the quark sources. For the point sources we use the lattice spacing a as source width R . Results for dynamical quarks: A (circles), B (squares), C (diamonds).

8 Conclusion

In this paper we have defined and calculated the chiral and partial wave content of the $\bar{q}q$ component of the ρ -meson at different resolution scales. We have used a complete (in terms of chiral symmetry) basis of interpolators that allows to define the chiral symmetry content of the quark-antiquark component of the ρ -meson. We have studied this in lattice simulations in the quenched limit as well as for configuration obtained with $n_f = 2$ dynamical, mass-degenerate light quarks. We have computed the cross-correlation matrix of the interpolators and applied the variational method for our analysis. The eigenvectors of the cross-correlation matrix supply us then with the direct information about decomposition of the quark-antiquark component of the ρ -meson in terms of different representations of the chiral group.

Given such a decomposition we were able, using the unitary transformation from the chiral basis to the LSJ -basis, to reconstruct the partial wave decomposition of the ρ -meson at different resolution scales. It turns out that at low resolution scales $R \sim 0.2 - 0.6$ fm the quark-antiquark component of the ρ -meson is a strong mixture of two representations of the chiral group $(0, 1) \oplus (1, 0)$ and $(1/2, 1/2)_b$ and consequently the chiral symmetry is strongly broken at these infrared scales. Only at the deep ultraviolet scale asymptotic freedom requires that the composition of the ρ -meson is determined

by the $(0, 1) \oplus (1, 0)$ representation alone. Consequently, at low resolution $R \sim 0.2 - 0.6$ fm the ρ wave function is predominantly 3S_1 wave with a tiny admixture of the 3D_1 wave depending on the scale. Only in the deep ultraviolet the ρ is given by the fixed $\sqrt{2/3}|I = 1; {}^3S_1\rangle + \sqrt{1/3}|I = 1; {}^3D_1\rangle$ superposition of the S - and D -waves with a sizeable contribution of the D -wave. This explains successes of the $SU(6)$ flavor-spin-symmetry for the ρ -meson, that explicitly relies on the 3S_1 content of the ρ wave function. Note, however, that we observe a resolution scale dependence of the composition, whereas the quark model does not.

Acknowledgement

We thank G. Engel, C. Gatttringer and D. Mohler for discussions. L.Ya.G. and M.L. acknowledge support of the Fonds zur Förderung der Wissenschaftlichen Forschung (P19168-N16) and (DK W1203-N08), respectively. C.B.L. acknowledges support by DFG project SFB/TR-55. The calculations have been performed on the SGI Altix 4700 of the Leibniz-Rechenzentrum Munich and on local clusters at ZID at the University of Graz.

References

- [1] F. Gürsey, L. A. Radicati, Phys. Rev. Lett. **13** (1964) 173.
- [2] J. J. J. Kokkedee, The Quark Model, W.A. Benjamin, NY, 1969 (and papers reprinted therein).
- [3] S. Aoki *et al.*, Phys. Rev. Lett. **82**, 4392 (1999), hep-lat/9901019.
- [4] M. B. Parappilly *et al.*, Phys. Rev. D **73**, 054504 (2006), hep-lat/0511007.
- [5] C. Michael, Nucl. Phys. B **259**, 58 (1985).
- [6] M. Lüscher and U. Wolff, Nucl. Phys. B **339**, 222 (1990).
- [7] L. Y. Glozman, Phys. Lett. B **587**, 69 (2004), hep-ph/0312354.
- [8] L. Y. Glozman, Phys. Rep. **444**, 1 (2007), hep-ph/0701081.

- [9] L. Y. Glozman and A. V. Nefediev, Phys. Rev. D **76**, 096004 (2007), arXiv:0704.2673 [hep-ph].
- [10] L. Ya. Glozman, C. B. Lang and M. Limmer, to appear in Phys. Rev. Lett. (2009), arXiv:0905.0811 [hep-lat].
- [11] T. D. Cohen and X. Ji, Phys. Rev. D **55**, 6870 (1997)
- [12] A. Lichtl, PoS **LATTICE2007**, 118 (2007), arXiv:0711.4072 [hep-lat].
- [13] C. Gattringer, L. Y. Glozman, C. B. Lang, D. Mohler, and S. Prelovsek, Phys. Rev. D **78**, 034501 (2008), arXiv:0802.2020 [hep-lat].
- [14] B. Blossier, M. DellaMorte, G. von Hippel, T. Mendes, and R. Sommer, JHEP **0904**, 094 (2009), arXiv:0902.1265 [hep-lat].
- [15] T. Burch, C. Hagen, C. B. Lang, M. Limmer, and A. Schäfer, Phys. Rev. D **79**, 014504 (2009), arXiv:0809.1103 [hep-lat].
- [16] D. Becirevic, V. Lubicz, F. Mescia, and C. Tarantino, JHEP **0305**, 007 (2003), hep-lat/0301020.
- [17] V. M. Braun *et al.*, Phys. Rev. D **68**, 054501 (2003), hep-lat/0306006.
- [18] C. Allton *et al.*, Phys. Rev. D **78**, 114509 (2008), arXiv:0804.0473 [hep-lat].
- [19] T. Burch and C. Ehmman, Nucl. Phys. A **797**, 33 (2007), hep-lat/0701001.
- [20] S. Güsken *et al.*, Phys. Lett. B **227**, 266(1989).
- [21] C. Best *et al.*, Phys. Rev. D **56**, 2743 (1997), hep-lat/9703014.
- [22] C. Gattringer, Phys. Rev. D **63**, 114501 (2001), hep-lat/0003005.
- [23] C. Gattringer, I. Hip, and C. B. Lang, Nucl. Phys. B **597**, 451 (2001), hep-lat/0007042.
- [24] C. Gattringer *et al.*, Nucl. Phys. B **677**, 3 (2004), hep-lat/0307013.
- [25] T. Burch *et al.*, Phys. Rev. D **70**, 054502 (2004), hep-lat/0405006.

- [26] T. Burch *et al.*, Phys. Rev. D **73**, 094505 (2006), hep-lat/0601026.
- [27] C. Gattringer *et al.*, Phys. Rev. D **79**, 054501 (2009), arXiv:0812.1681 [hep-lat].
- [28] M. Lüscher and P. Weisz, Commun. Math. Phys. **97**, 59 (1985).